Engineering Transactions, **69**(3): 257–269, 2021, doi: 10.24423/EngTrans.1265.20210826
Polish Academy of Sciences • Institute of Fundamental Technological Research (IPPT PAN)
Université de Lorraine • Poznan University of Technology

Research Paper

A Computational Analysis of Different Geometric Ratios at the Input of a Secondary Fluid that Affects the Efficiency of a Subsonic Air-Air Ejector

Jhon Fredy HINCAPIE-MONTOYA[1)], Jorge Andres SIERRA-DEL-RIO[2)], Edwar TORRES-LOPEZ[3)], Diego Andres HINCAPIE-ZULUAGA[2)*]

[1)] *Department of Engineering, Research Group – GIIAM*
Institución Universitaria Pascual Bravo
Medellín, Colombia

[2)] *Department of Mechatronic Engineering, Research Group – MATyER*
Instituto Tecnológico Metropolitano
Medellín, Colombia
*Corresponding Author e-mail: diegohincapie@itm.edu.co

[3)] *Department of Mechanical Engineering, Research Group – GEA*
Universidad de Antioquia
Medellín, Colombia

For this study, the computational fluid dynamics (CFD) technique was used to investigate the combined effects of different geometric parameter relationships; inclination angle variation of the secondary fluid inlet, different lengths of the mixing chamber, and different separation values between the nozzle outlet and the input of the mixing chamber, in an air-air ejector used in a subsonic regime. As a working fluid, the air was used as an ideal gas and its viscosity was expressed as a constant both in the primary and secondary fluids. The renormalization group (RNG) $\kappa-\varepsilon$ turbulence model was used to predict more accurately the way the pressure recovers along the ejector and suitability/applicability to for recirculation flows. It was found in the numerical results that there is an optimal value of the inclination angle for the secondary fluid inlet, the length of the mixing chamber and the separation between the nozzle outlet and the mixing chamber inlet, where the ejector obtains its maximum mass flow ratio. In addition, it was found that the efficiency of the air-air ejector is related to the inclination angle of the secondary fluid inlet.

Key words: ejector; geometric parameters; subsonic flow; CFD; Ansys Fluent.

1. Introduction

Ejectors are static pumping devices that use the kinetic energy of a primary fluid to create a low pressure and drag a secondary fluid. They are made up

of four parts: nozzle, suction chamber, mixing chamber and diffuser [1]. The primary fluid leaves the nozzle at high velocity and drags a secondary fluid from the surroundings of the nozzle, called the suction chamber. The suction chamber can be of two types: axial input or circumferential input. The mixing process of the two fluids takes place in the constant cross-sectional area, called the mixing chamber. In the diffuser, at the end of the mixing chamber, the mixture slows down to the discharge velocity and pressure, see Fig. 1. The ejector's advantages lie in simple construction, easy installation, low cost and no moving parts, so it does not require periodic maintenance.

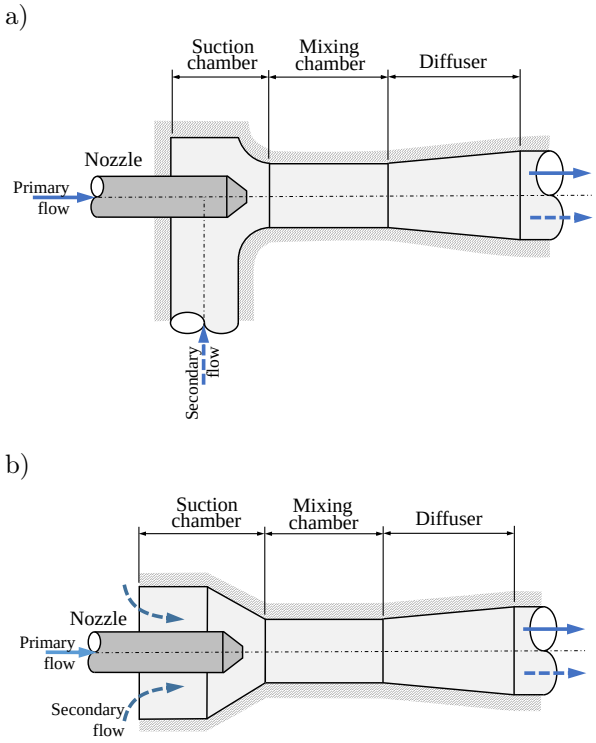

Fig. 1. Ejector diagram: a) ejectors with axial inlet suction chamber, b) ejectors with circumferential inlet suction chamber.

The ejectors are crucial for industrial processes such as: corrosive liquid pumping, nuclear reactor cooling systems, steam compression cooling systems, and industrial ventilation in power plants, in which, due to the operating conditions, the implementation of traditional ventilation equipment becomes unfeasible [2–4]. Therefore, the high efficiency of the device is critical. The ejector efficiency is defined as the amount of energy transferred from the secondary fluid to the primary fluid.

Experimental studies have been conducted about the efficiency of the air-air ejectors by changing its geometric parameters: a mixing chamber length, the separation between nozzle outlet and mixing chamber inlet, and the diffuser angle. In addition to these geometrical parameter changes, MEAKHAIL *et al.* [5] increased the number of nozzles in the ejector. They found that changing the number of nozzles in the ejector does not have a notable effect on its efficiency. FLOREAN *et al.* [6] made measurements of the velocities and their fluctuations using the f particle image velocimetry (PIV) in the mixing chamber for three different geometries of a jet pump. On the other hand, AISSA [7] worked with sonic and supersonic ejectors, where the secondary fluid entered the mixing chamber through two coaxial tubes to the nozzle. Experimental results showed that low-pressure ratio ejectors have a higher efficiency than high-pressure ratio ejectors. However, in these experimental studies, the secondary fluid was circumferentially introduced into the suction chamber and was supplied by an air compensation tank that controlled and measured the flow rate entered, regardless of the geometric parameters of the secondary fluid inlet and suction chamber.

Nowadays, the application of computational tools is required to test, modify and analyze geometric parameters that can influence the efficiency of ejectors. The computational fluid dynamics (CFD) technique provides more detailed information on complex phenomena taking place in ejectors. For example, MANZANO *et al.* [8] used this technique to determine the influence that the geometry of a Venturi injector's geometry on the pressure losses for different throat morphologies. They demonstrated that using rounded edges in the suction chamber would delay the development of cavitation and reduce pressure losses. LISOWSKI and MOMENI [9] performed CFD simulations of the fluids present in a new prototype jet pump. They evaluated three different nozzle designs, and presented their influence on the ejector pressure head. LIU and COSTIGAN [10], using CFD, modeled the formation of supersonic swirling flows in a prototype ejector. GENC *et al.* [11] conducted CFD simulations to investigate the influence of the inclination angle of the secondary fluid on the performance of ejectors used in solid oxide fuel cells. They found that the resistance of the primary fluid decreases by increasing the inclination angle of the secondary fluid, therefore, improving ejectors' performance. Through the conducted CFD simulations, they concluded that the swirling effect helps in mixing the flows, decreasing the central velocity and increasing velocity near the walls of the prototype ejector.

Experimental and CFD work has been carried out on different geometric parameters separately in the ejectors, and similar results in air-air subsonic ejector efficiency performance were obtained. However, few articles present CFD investigations of subsonic ejectors with different geometric parameters at the secondary fluid inlet.

In this work, the efficiency of an air-air subsonic ejector was studied by CFD, considering the combination of different geometric parameter relationships: the variation of the inclination angle of the secondary fluid inlet, for different lengths of the mixing chamber versus its diameter, and the separation between nozzle outlet and mixing chamber inlet versus the injector diameter. In addition, experimental work is carried out that is mainly used for the validation of the model by CFD.

2. Ejector modeling

2.1. Ejector geometric parameters

The subsonic ejector model used in this work is shown in Fig. 2. The main parts of the ejector are the suction chamber with an axial inlet at an inclination angle of β, the mixing chamber with a length L_{mc} and a constant diameter D_{mc}, and the converging nozzle with an outlet diameter d_p. Additionally, there is the separation H between nozzle outlet and mixing chamber inlet. By the point p, a primary fluid enters at a pressure P_p and with a volumetric flow of Q_p. The primary fluid leaves the nozzle at point o, creating a low-pressure region in the nozzle outlet and around the suction chamber. Because of this, the secondary fluid is dragged freely, from point s, at a pressure P_s and with a volumetric flow of Q_s. The entrained secondary fluid mixes with the primary fluid in the mixing chamber. The mixture leaves by point d, with a discharged pressure P_d with a volumetric flow Q_d. In this work, the diffuser was not used at the end of the mixing chamber.

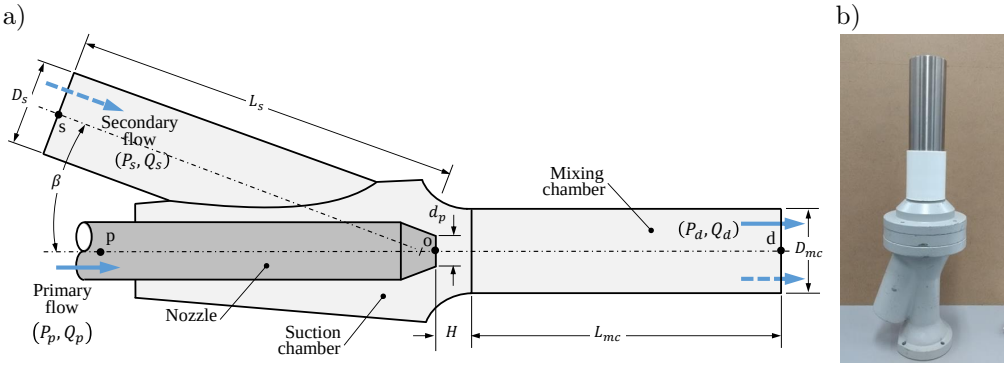

Fig. 2. Subsonic ejector representation: a) geometrical parameters, b) commercial ejectors.

The main geometric parameters of the commercial ejector used in this work are the inclination angle of the secondary fluid inlet towards the suction chamber, $\beta = 20°$, the mixing chamber diameter, $D_{mc} = 43.9$ mm, the nozzle outlet

diameter, $d_p = 15.76$ mm, and finally, the separation between the nozzle outlet and mixing chamber inlet, $H = 97$ mm. For the mixing chamber length L_{mc}, a stainless-steel tube of the same diameter coupled to the ejector was used.

The performance of air-air ejectors is presented in the form of the mass flow ratio of secondary fluid and primary fluid (ϕ) versus pressure ratio (R_p), from the axial suction inlet to the mixing chamber outlet. The efficiency of air-air ejectors was calculated by CHOU [1] using the following equation:

$$\eta = \frac{\rho_s Q_s \left(P_d - P_s\right)}{\rho_i Q_i \left(P_i - P_d\right)} \cdot 100 = \phi R_p. \tag{2.1}$$

2.2. Experimental method

The schematic diagram of the experimental system used in this study, which includes the air supply unit and its measuring instruments, is shown in Fig. 3. For the primary fluid line, a centrifugal fan is used to enter a constant air volumetric flow rate. The pressure and volumetric flow rate of the primary fluid are adjusted by the valve. While for the secondary fluid line, the pressure is atmospheric and the volumetric flow is dragged on demand. An anemometer was installed at the mixing chamber outlet to quantify the outlet velocity of the mixture.

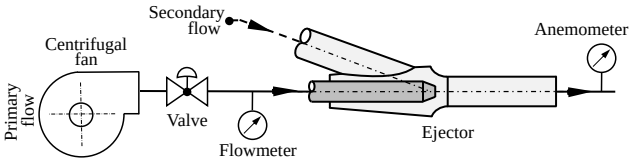

FIG. 3. The schematic diagram of the experimental system.

The CFD analysis consisted of combining three different geometric parameter relationships of the ejector. The first relationship refers to the inclination angle of the secondary fluid inlet versus the suction chamber, where the angle took the values between $20° \leq \beta \leq 90°$. The second relationship refers to the mixing chamber length versus the mixing chamber diameter, where five relationships were used: $L_{cm}/D_{cm} = 2, 4, 6, 8, 10$. Moreover, the third relationship refers to the separation between the nozzle outlet and mixing chamber inlet versus the injector diameter, where three relationships were used: $H/d_p = 0, 1, 2$.

3. CFD MODEL

All governing CFD equations for the air-air subsonic ejector, turbulent and three-dimensional in steady-state, were performed as follows.

3.1. Mathematic model

The continuity, momentum and energy equations for stable state flow used to solve the system are shown below:

$$\frac{\partial U_i}{\partial x_i} = 0, \tag{3.1}$$

$$\rho U_j \frac{\partial U_i}{\partial x_j} = -\frac{\partial P}{\partial x_i} + \frac{\partial}{\partial x_j}\left[\mu_{\text{eff}}\left(\frac{\partial U_i}{\partial x_j} + \frac{\partial U_j}{\partial x_i}\right) - \rho\overline{u_i' u_j'}\right], \tag{3.2}$$

$$\rho U_j \frac{\partial T}{\partial x_j} = \frac{\partial}{\partial x_j}\left[\frac{\mu}{\text{Pr}}\frac{\partial T}{\partial x_j} - \rho\overline{T' u_j'}\right], \tag{3.3}$$

where U, P and T are the components of velocity, pressure and temperature; u_i' and T' are the fluctuant components of the velocity and temperature; ρ, μ_{eff} and Pr are density, effective dynamic viscosity and Prandtl number of the fluid, respectively. Effective dynamic viscosity is equal to $\mu_{\text{eff}} = \mu + \mu_T$, where, turbulent viscosity μ_T is calculated by $\mu_T = C_\mu \rho \left(\kappa^2/\varepsilon\right)$.

Turbulent stress tensor $-\rho\overline{u_i' u_j'}$ was calculated by the RNG $\kappa - \varepsilon$ turbulence model [12]. Among Reynolds-averaged Navier-Stokes (RANS) turbulence models, the RNG $\kappa - \varepsilon$ model can more accurately predict pressure recovery along the ejector and is suitable for flows with recirculation [13, 14]. The equations that model turbulent kinetic energy κ and the dissipation ratio ε are as follows:

$$\frac{\partial}{\partial x_j}\left(\rho U_j \kappa\right) = \frac{\partial}{\partial x_j}\left[\alpha_\kappa \mu_{\text{eff}} \frac{\partial \kappa}{\partial x_j}\right] + G - \rho\varepsilon, \tag{3.4}$$

$$\frac{\partial}{\partial x_j}\left(\rho U_j \varepsilon\right) = \frac{\partial}{\partial x_j}\left[\alpha_\varepsilon \mu_{\text{eff}} \frac{\partial \varepsilon}{\partial x_j}\right] + C_1 \frac{\varepsilon}{\kappa} G - \rho C_2 \frac{\varepsilon^2}{\kappa}, \tag{3.5}$$

where α_κ and α_ε are the inverse effective Prandtl numbers for κ and ε, respectively. The turbulent kinetic energy production ratio G is calculated by

$$G = \mu_T \left(\frac{\partial U_j}{\partial x_k} + \frac{\partial U_k}{\partial x_j}\right)\frac{\partial U_j}{\partial x_k}, \tag{3.6}$$

the RNG $\kappa - \varepsilon$ turbulence model assumes different values for the coefficients, evaluated by the standardization group theory as follows:

$$C_2 = 1.68 + \frac{C_\mu n^3 \left(1 - (n/4.8)\right)}{1 + 0.012 n^3}, \tag{3.7}$$

with $n = \frac{\kappa S}{\varepsilon}$ and $S = \sqrt{2 S_{jk} S_{jk}}$, where n is the turbulent average stress timeline and $\mathbf{S}$ is the tensor of the average deformation rate. The constant parameters of the RNG $\kappa - \varepsilon$ turbulence model are given by $C_\mu = 0.0845$, $C_1 = 1.42$, and $\sigma_\kappa = \sigma_\varepsilon = 0.7194$.

3.2. Numeric solution

Continuity, momentum, energy and turbulence equations were solved using ANSYS FLUENT software based on the finite volume method. In all cases, air as an ideal gas was used as a working fluid and its viscosity was expressed constant due to small temperature changes in the ejector. To solve these equations, appropriate boundary conditions must be applied on each of the ejector surfaces. At the inlet of the nozzle, the primary fluid is with a constant mass flow equal to 0.031 kg/s. A static pressure inlet condition was implemented at the mixing chamber inlet. Meanwhile, a static pressure outlet condition was implemented at the mixing chamber outlet. The adiabatic boundary condition and non-slip without roughness were implemented on all ejector walls. The flow near the walls was treated with standard wall functions.

The computational domain was discretized using a structured mesh. The size and number of elements along the central axis of the nozzle and mixing chamber were controlled, better capturing the secondary fluid entrainment and the mixture in the mixing chamber. The mesh size for the whole ejector was exploited to improve accuracy and computation time, see Fig. 4.

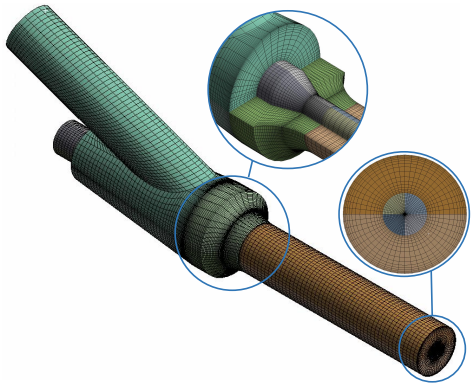

FIG. 4. Details of the ejector's computational domain structured mesh.

The number of elements used in the computational domain has a strong influence on the obtained results. Therefore, a mesh independence analysis was carried out to ensure the accuracy and reliability of the results in a shorter calculation time. The pressure and velocity at point s, at the secondary fluid inlet, and at point d, at the mixing chamber outlet, are used to perform the independence analysis. In addition, the computational model was validated by comparing the mass flow ratio, ϕ, experimentally obtained and by CFD. In Table 1 it can be seen that errors are very close to each other, and with 308 660 elements, the most acceptable errors for the three comparisons are obtained.

Table 1. Analysis of mesh independence and verification of results at points s and d.

Number of cells	Point s				Point d				ϕ Exp.	ϕ CFD	Error [%]
	Pressure [Pa]	Error [%]	Velocity [m/s]	Error [%]	Pressure [Pa]	Error [%]	Velocity [m/s]	Error [%]			
210 544	100 768	–	31.61	–	101 303	–	71.67	–		–	–
244 760	100 754	0.01389	31.19	1.3354	101 300	0.00296	71.50	0.232		0.2884	0.5597
288 436	100 752	0.00199	31.18	0.0093	101 300	0.00000	71.27	0.332	0.29	0.2897	0.1138
308 660	100 752	0.00000	31.12	0.1927	101 300	0.00000	71.15	0.163		0.2899	0.0276
329 944	100 737	0.01489	30.73	1.2479	101 299	0.00099	70.39	1.066		0.2894	0.2052

4. Results and discussion

To investigate the geometric parameter relationships of the air-air ejector in regard to its performance and efficiency, a series of CFD simulations were performed based on the mathematical model mentioned above. The results are presented as follows.

4.1. Effect of mixing chamber length

Geometric parameters of the mixing chamber are critical to obtain a better mass flow ratio in the ejector, especially because this is where the mixture of primary fluid and secondary fluid carried on demand occurs, and large changes in velocity occur along the axis. For a single inclination angle of the secondary fluid input $\beta = 20°$, the variation of the mass flow ratio ϕ with the mixing chamber length ratio versus the diameter of the mixing chamber L_{cm}/D_{cm}, for three different separation ratios between the nozzle outlet and mixing chamber inlet versus the injector diameter $H/d_p = 0$, 1, 2, and for a single inclination angle of the secondary fluid input $\beta = 20°$, are is shown in Fig. 5.

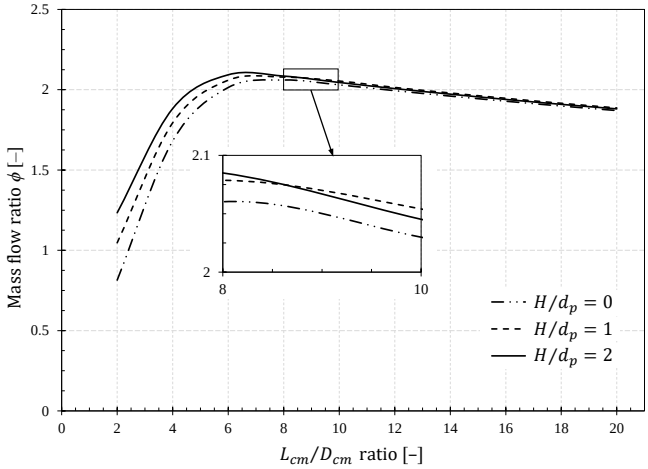

Fig. 5. Comparison of the mass flow ratio for relationship L_{cm}/D_{cm} for different ratios of H/d_p.

For the three H/d_p ratios, increasing the L_{mc}/D_{mc} ratio increases the mass flow ratio to a maximum mass flow value. It can be seen that there is an optimal range for the L_{mc}/D_{mc} ratio so that the ejector reaches its maximum mass flow ratio. The maximum mass flow ratio for all three H/d_p ratios was found around $L_{cm}/D_{cm} \approx 7$. For $L_{cm}/D_{cm} < 7$ ratios, the mass flow ratio increases for the three H/d_p ratios, because a longer length helps to mix fluids better, therefore their kinetic energy exchanges more efficiently. For the $L_{cm}/D_{cm} > 7$ ratios, the mass flow ratio slightly decreases, for the three H/d_p ratios, because friction losses increase along the mixing chamber. Previous research suggested that the maximum mass flow ratio is in a range of $5 < L_{cm}/D_{cm} < 10$ [15, 16].

Another notable trend observed in the results is that for $L_{cm}/D_{cm} < 7$ ratios, the mass flow ratio increases at a greater ratio of H/d_p. Meanwhile, in the $L_{cm}/D_{cm} > 7$ ratios, there is no significant increase in the mass flow ratio by increasing the H/d_p ratio, so a part of Fig. 5 is enlarged to see this behavior better.

4.2. Inclination angle effect (secondary fluid)

The geometric parameters of the secondary fluid inlet are mainly the tube inlet diameter D_s, length of the tube L_s, and an inclination angle of the secondary fluid input β. In this work, the geometric parameters D_s and L_s for the secondary fluid input remained constants. The variation in the ejector efficiency η with the variation of the inclination angle between $20^\circ < \beta < 90^\circ$, with the mixing chamber length ratio versus the mixing chamber diameter, $L_{cm}/D_{cm} = 2$, 4, 6, 8, 10, and the separation between nozzle outlet and mixing chamber inlet versus of the injector diameter, $H/d_p = 0$, 1, 2, are shown in Fig. 6.

For the H/d_p ratios, by increasing the inclination angle at the secondary fluid inlet β from 20° to 90°, the ejector efficiency decreases significantly, around $\approx 25\%$, for all the L_{mc}/D_{mc} relationships, because it increases the passage resistance of the secondary fluid. By increasing the H/d_p ratio, for the $L_{mc}/D_{mc} = 2,\ 4$ ratios, the efficiency increases significantly. For the $L_{mc}/D_{mc} = 6,\ 8,\ 10$ ratios, there is no significant increase in efficiency because the L_{mc}/D_{mc} ratio is close to its maximum efficiency value (maximum mass flow ratio).

4.3. Ejector velocities features

The velocities contours in the ejector of the primary, secondary fluids and the mixture of them in the mixing chamber are caused by the high velocity with which the primary fluid leaves the nozzle. The variation of the ejector velocity contours for different inclination angles β, where $L_{mc}/D_{mc} = 6$ and $H/d_p = 0$, are shown in Fig. 7.

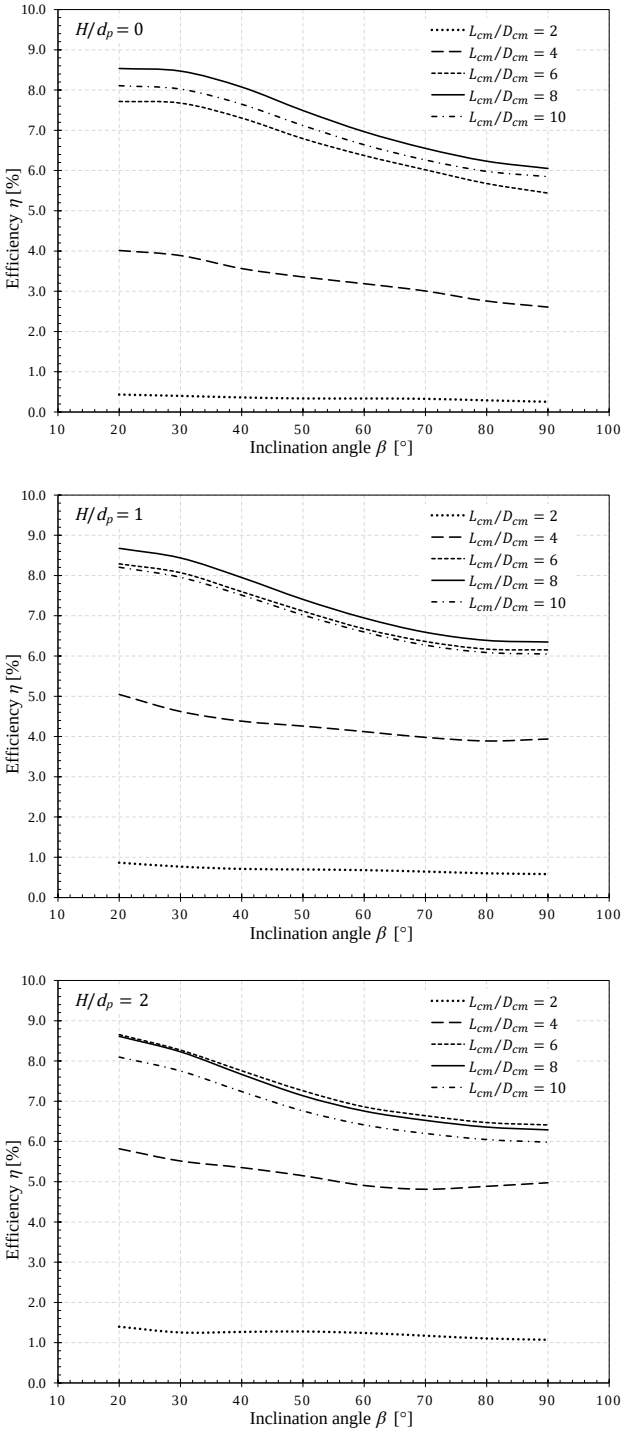

FIG. 6. Comparison of the variation of the inclination angle *versus* H/d_p ratios.

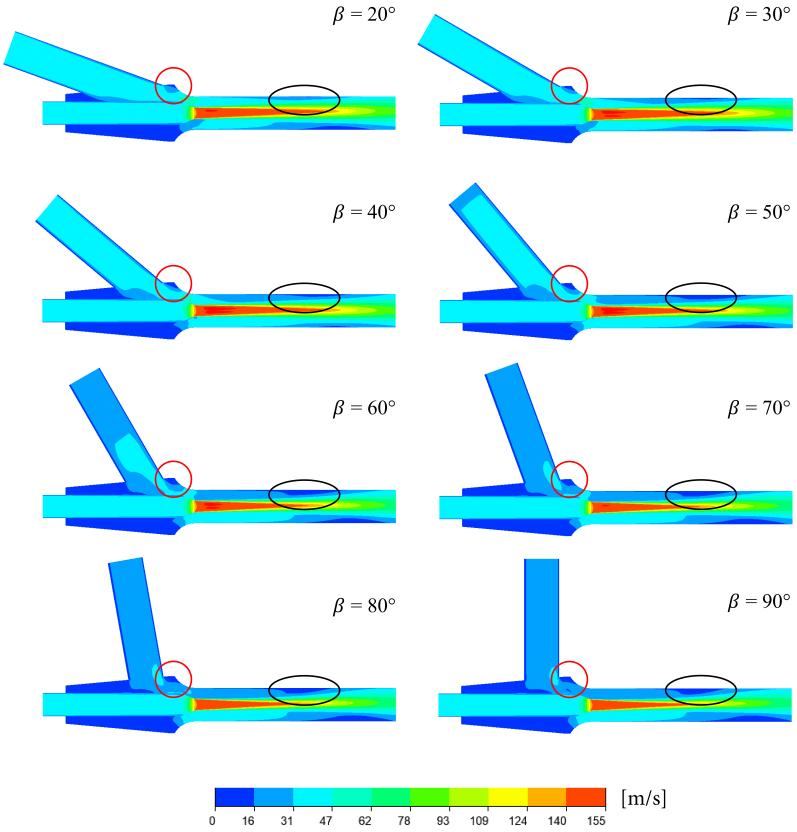

FIG. 7. Ejector velocity contours depending on the tilt angle, the display of recirculation zones.

In the ejector, the highest velocities are at the nozzle outlet, 155.15 m/s. Then, the velocities decrease in the mixing chamber, and the exchange of kinetic energy between the primary and secondary fluids is done. For the secondary fluid velocity, there is a reduction as the inclination angle β increases. The average velocity at the inlet of the inclined tube for a $\beta = 20°$ is 32.11 m/s, and for a $\beta = 90°$ is 28.4 m/s, due to the passage resistance of the secondary fluid. It is observed that the distribution of velocities in the mixing chamber is asymmetrical with respect to the central axis of the nozzle.

The secondary fluid is influenced by the inclination angle β and by the inner walls of the mixing chamber, where recirculation zones occur (see Fig. 7, red circle) in the lower part of the secondary tube, and a second circulation zone (see Fig. 7, black circle) occurs around the middle of the mixing chamber. These recirculation zones become larger as the inclination angle β increases. This increases friction between the primary fluid and the secondary fluid, increases the loss of kinetic energy, and decreases ejector efficiency.

5. Concluding remarks

In this work, CFD simulations were performed to study the influence of geometric parameters, the inclination angle of the suction chamber inlet, the mixing chamber length versus its diameter, the separation between the nozzle outlet and the mixing chamber inlet versus the injector diameter, in the mass flow ratio and the air-air subsonic ejector efficiency.

The analysis for the different geometrical relationships shows an optimum value of the mixing chamber length and the separation between the nozzle outlet and the mixing chamber inlet, where the ejector obtains its maximum mass flow ratio and efficiency. Before this optimum value, every geometrical change causes a big change in the mass flow ratio and ejector efficiency. After this optimum value the mass flow radio and ejector efficiency tend to remain invariant. Additionally, it was found that by increasing the inclination angle of the secondary fluid inlet to the suction chamber, the efficiency of the ejector decreases by approximately 25% for all geometric relationships. Also, the recirculation zones in the lower part of the secondary tube and in the mixing chamber, for the secondary fluids and the fluid mixture, are greater when this angle is increased.

References

1. Chou S.K., Experimental studies on an air-air jet exhaust pump, *ASHRAE Transactions (United States)*, **92**(2A): 497–506, 1986.

2. Li F. *et al*, Experimental determination of the water vapor effect on subsonic ejector for proton exchange membrane fuel cell (PEMFC), *International Journal of Hydrogen Energy*, **42**(50): 29966–29970, 2017, doi: 10.1016/j.ijhydene.2017.06.226.

3. Chunnanond K., Aphornratana S., Ejectors: applications in refrigeration technology, *Renewable and Sustainable Energy Reviews*, **8**(2): 129–155, 2004, doi: 10.1016/j.rser.2003.10.001.

4. Cępa P., Lisowski E., Application of pneumatic suction cup as a positioning element for thin metal sheets in technological processes, *Technical Transactions; Mechanics*, **2013**(1-M (5)): 5–12, 2013, doi: 10.4467/2353737XCT.14.001.1927.

5. Meakhail T.A., Zien Y., Elsallak M., AbdelHady S., Experimental study of the effect of some geometric variables and number of nozzles on the performance of a subsonic air-air ejector, *Proceedings of the Institution of Mechanical Engineers, Part A: Journal of Power and Energy*, **222**(8): 809–818, 2008, doi: 10.1243/09576509JPE618.

6. Florean F.G., Petcu A.C., Porumbel I., Dediu G., PIV measurements in low noise optimized air jet pump demonstrators, *International Journal of Energy*, **10**: 33–43, 2016.

7. Aissa W.A., Performance analysis of cylindrical type air ejector, *JES. Journal of Engineering Sciences*, **34**(3): 733–745, 2006, doi: 10.21608/jesaun.2006.110609.

8. Manzano J. Palau C.V., de Azevedo Benito M., do Bomfim Guilherme V., Vasconcelos D.V., Geometry and head loss in Venturi injectors through computa-

tional fluid dynamics, *Engenharia Agrícola*, **36**(3): 482–491, 2016, doi: 10.1590/1809-4430-Eng.Agric.v36n3p482-491/2016.

9. Lisowski E., Momeni H., CFD modeling of a jet pump with circumferential nozzles for large flow rates, *Archives of Foundry Engineering*, **10**(3): 69–72, 2010.

10. Liu Y., Costigan G., CFD simulations of swirling effects on the performance of the supersonic nozzle for micro-particle delivery, [in:] *Proceedings of the 5th WSEAS International Conference on Applied Computer Science*, Hangzhou, China, April 16–18, 2006, pp. 584–589, 2006.

11. Genc O., Timurkutluk B., Toros S., Performance evaluation of ejector with different secondary flow directions and geometric properties for solid oxide fuel cell applications, *Journal of Power Sources*, **421**: 76–90, 2019, doi: 10.1016/J.JPOWSOUR.2019.03.010.

12. Yakhot V., Orszag S.A., Thangam S., Gatski T.B., Speziale C.G., Development of turbulence models for shear flows by a double expansion technique, *Physics of Fluids A: Fluid Dynamics*, **4**(7): 1510–1520, 1992, doi: 10.1063/1.858424.

13. Bartosiewicz Y., Aidoun Z., Desevaux P., Mercadier Y., CFD-experiments integration in the evaluation of six turbulence models for supersonic ejectors modeling, [in:] *Proceedings of Integrating CFD and Experiments Conference*, Glasgow, UK, 2003.

14. Taherian M., Saedodin S., Valipour M.S., Numerical simulation of subsonic jet ejector, *Journal of Modeling in Engineering*, **14**(45): 63–78, 2016, doi: 10.22075/jme.2017.1763.

15. Winoto S.H., Li H., Shah D.A., Efficiency of jet pumps, *Journal of Hydraulic Engineering*, **126**(2): 150–156, 2000, doi: 10.1061/(ASCE)0733-9429(2000)126:2(150).

16. Chunnanond K., Aphornratana S., An experimental investigation of a steam ejector refrigerator: the analysis of the pressure profile along the ejector, *Applied Thermal Engineering*, **24**(2–3): 311–322, 2004, doi: 10.1016/j.applthermaleng.2003.07.003.

Received October 6, 2020; accepted version June 17, 2021.
